Journal of Metals, Materials and Minerals, Vol. 31, No. 1, pp. 73-80, 2021

Microstructure and properties of zirconia-alumina composites fabricated via powder injection molding

Nalattaporn SAELEE[1,*], Nutthita CHUANKRERKKUL[2], and Panitarn WANAKAMOL[1]

[1]*Department of Materials Science, Srinakharinwirot University, 114 Sukhumvit 23, Wattana, Bangkok, 10110, Thailand*
[2]*Metallurgy and Materials Science Research Institute, Chulalongkorn University, Soi Chulalongkorn 12, Wang Mai, Pathum Wan, Bangkok, 10330, Thailand*

***Corresponding author e-mail:** Nalattaporn.saelee@g.swu.ac.th

Received date:
31 December 2020
Revised date
29 January 2021
Accepted date:
6 February 2021

Keywords:
Powder injection molding;
Zirconia;
Alumina;
Flexural test;
X-ray diffraction

Abstract

This study aimed to fabricate zirconia-alumina composites via powder injection molding and investigate the effects of alumina addition on microstructure as well as physical properties of the composites. Zirconia-alumina composites were prepared using polyethylene glycol (PEG) and polyvinyl butyral (PVB) as binders. The powder loading was fixed at 38 vol%, and PEG: PVB binder weight ratio was fixed at 80:20. Alumina content within ceramic component was varied at 0, 10, 20, 30, 40 and 50 vol% to observe the effect of alumina on the composite structures and properties. The injection molding was done at 190°C followed by water debinding of PEG at 40°C. Thermal debinding of PVB at 450°C was performed prior to sintering at 1450°C. From the density measurement via Archimedes' method, the relative density of sintered samples was found to be highest at 10 vol% alumina and gradually lower at higher alumina content. The condition with highest density yielded the highest flexural modulus and flexural strength. XRD indicated that tetragonal zirconia phase coexisted with alumina when alumina was added. Above 20 vol% alumina, monoclinic zirconia was also detected. The increased porosity in samples with high alumina content, as confirmed in SEM morphological observation, correlated with lower flexural strength and lower flexural modulus. The results illustrated the feasibility of powder injection molding in the production of zirconia-alumina composites and the optimum condition in this study was 10 vol% alumina.

1. Introduction

Powder injection molding (PIM) is a fabrication process that allows metallic and ceramic materials to be molded into complex shapes. Metallic or ceramic powders are mixed with polymeric binder to create flowability when the mixture is heated above binder melting temperature. In the injection process, the mixture is heated and injected into a mold. Variables of considerations include powder size, powder-to-binder ratio, type of binder, injection temperature. Various metallic and ceramic powders have been fabricated into complex architecture via the powder injection method [1].

Zirconia is a high-performance ceramic with high strength and toughness. Its exceptional toughness is due to phase transformation toughening. To improve other mechanical properties of zirconia such as Young's modulus and hardness, alumina can be added into zirconia matrix to form zirconia-alumina ceramic composite or alumina-toughened zirconia (ATZ) with potential applications in dental restorative materials or implants [2-5]. Studies on the system have been done using simple fabrications such as tape casting and pressing. These studies showed that variation of constituent ratio leads to changes in mechanical properties [6-12]. None of the past studies has utilized PIM for the fabrication of alumina-toughened zirconia. Powder injection molding of zirconia [13-21] have been explored in a number of studies. Previous studies of zirconia powder injection molding illustrate that the molding method can shape zirconia into complex shapes such as micro gears and optical sleeves [14-18]. Most of zirconia PIM employed binders such as wax, polypropylene, polyethylene, and stearic acid that need to be debinded using organic solvents [19-21]. Fewer studies have investigated zirconia-toughened alumina PIM [22-24].

This work explored the feasibility of powder injection molding on fabrication of zirconia-alumina composites with zirconia as major component, and studied the effect of alumina addition on microstructure and physical properties of the injection molded samples.

2. Experimental

2.1 Sample preparation

Zirconia-alumina composite samples were prepared via powder injection molding. The feedstock was made up of zirconia powder (3 mol% yttria stabilized zirconia (TZ-3YE) obtained from TOSOH Cooperation), alumina powder (A32 from Nippon Light Metal Co., Ltd.) and polymeric binders. The powder-to-binder ratio was fixed at 38:62 by volume. This ratio was preliminarily tested to assure flowability of the majority phase, zirconia. The binders consisted of 80 wt% of

polyethylene glycol (PEG) and the 20 wt% of polyvinyl butyral (PVB). PEG enabled the powder to flow smoothly in the mold cavity and can be removed with water. PVB functioned as backbone binder to keep the shape of molded piece firm [25]. The density information for the precursors are in Table 1. For this study, we varied alumina content at 0, 10, 20, 30, 40 and 50 vol% of the ceramic powder content such that the sample names were A0, A10, A20, A30, A40 and A50. The comparison between weight composition and volume composition of the powder component is provided in Table 2, as some studies might refer to composition as weight ratio. Prior to mixing, the ceramic powders were sieved and dried at 100℃ for 10 h to get rid of moisture. The powders mixture was prepared through the following steps. First, zirconia and alumina powders were mixed in ball mills at 200 rpm for 20 min. The combined powders were mixed with PVB using ethanol. The mixture paste was dried overnight on an aluminum foil at the room temperature. The dried paste was then crushed and then melted over a hotplate at 60℃ for 8 min before mixing thoroughly with molten PEG. To homogenize the feedstock, the whole mixture was injected repeatedly for 9 times for mixing purpose before final injection into a mold. Injection molding process was performed using a plunger-type machine. The shape of the mold was a rectangular bar with dimension 5 x 5 x 56 mm^3. The injection temperature was set at 190°C. To remove polymeric binders, PEG was leached out in 40℃ water bath for at least 1 day. The leaching experiment was also performed at different time intervals from 30 min to 6 h to observe how leaching progressed. After each time interval, the samples were dried at room temperature for 1 day before they were weighed to obtain PEG removal percentage. The thermal treatment of the specimens combined thermal debinding of PVB and sintering step into one process. The heat treatment profile is depicted in Figure 1. The samples were held at 450℃ for 1 h for thermal debinding followed by sintering at 1450℃ for 2 h.

2.2 Characterization

Sample characterizations included density measurement, x-ray diffraction, mechanical tests and microstructure analysis.

Density. Density of sintered samples were measured using Archimedes' method, which allowed bulk density and porosity to be calculated.

X-ray diffraction analysis. Phase composition of zirconia-alumina composites samples were probed under Bruker AXS model D3 Discover. The sintered samples with different alumina content were cut into thin square pieces. The analyses were performed using Cu radiation with generator voltage (current) of 40 kV (40 mA). The scan angle ran from 20 to 100 degrees, at 0.002 degree/step.

Mechanical test. Three-point bending flexural test of sintered samples was performed using a universal testing machine (Instron 5882) according to ASTM C1161-02C, with a span of 25 mm.

Microstructure and chemical composition analysis. Fracture surface of sintered samples were characterized by scanning electron microscope (JEOL, JSM-IT300 Oxford X-Max20). The microscope was equipped with energy dispersive spectroscopy (EDS) mode that provided chemical composition of the viewed areas.

Table 1. Powders and binders used in sample fabrication and their densities.

Precursor substances	Density ($g \cdot cm^{-3}$)
Zirconia	6.05
Alumina	3.90
PVB	1.10
PEG	1.10

Table 2. Alumina content in ceramic component shown in volume% compared with weight%.

	Sample name					
	A0	**A10**	**A20**	**A30**	**A40**	**A50**
Alumina content in ceramic component (vol%)	0	10	20	30	40	50
Alumina content in ceramic component (wt%)	0.0	6.7	13.9	21.7	30.1	39.2

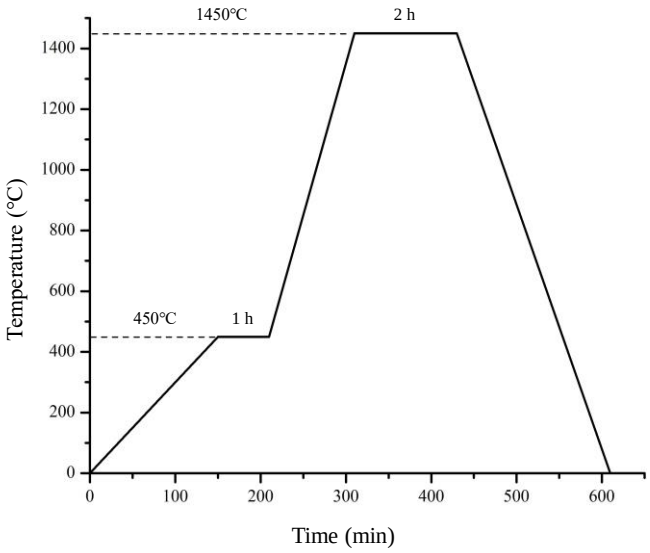

Figure 1. Heat treatment profile for thermal debinding and sintering process.

3. Results and discussion

Zirconia-alumina composites were fabricated from zirconia powder, alumina powder, PEG and PVB into rectangular pieces. Figure 2 depicts as-received ceramic powders and an injection molded specimen. After injection molding, the subsequent processes included water debinding and thermal debinding followed by sintering.

3.1 Water debinding of PEG and leached microstructure

The injected specimens which contained both ceramic particles and binders were first debinded in water. PEG, which can be dissolved in water, was leached out and eliminated in this step. To ensure the removal of PEG, leaching experiment was performed at different time durations. The plot of PEG removal vs. leaching time is shown in Figure 3. For all sample conditions, PEG was removed at high rates initially.

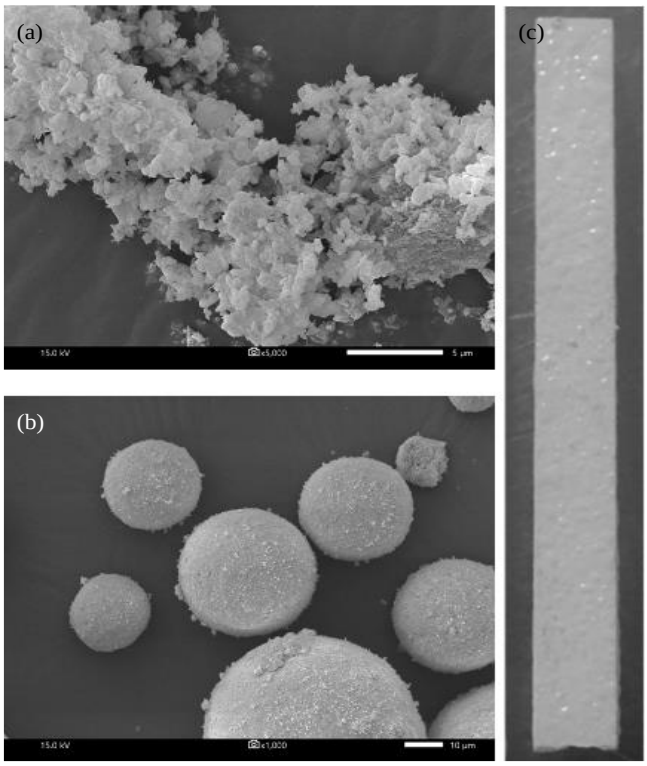

Figure 2. As-received alumina powder (a), zirconia powder (b), and an as-injected zirconia-alumina composite specimen (c).

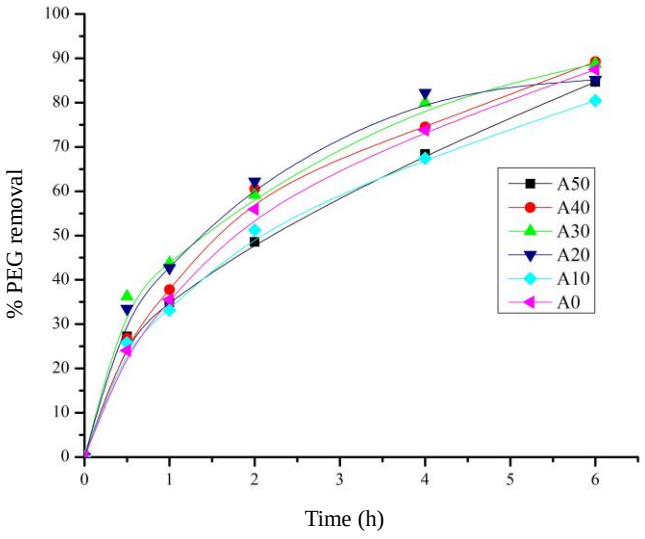

Figure 3. PEG removal vs. leaching time for composite samples with various alumina content.

PEG diffusion off from the samples tended to be fast in the initial stage because PEG at sample surface directly interacted with water. With longer leaching time, the removal rates became lower, because the remaining PEG within the samples took longer path to diffuse out. After 24 h of leaching time, PEG was completely eliminated from all the samples. PEG removal step would leave pores in the sample such that PVB could escape out in the thermal debinding process through these pores [26-28].

Figure 4(a) and 4(b) illustrate surface evolution of the six specimen conditions, A0 to A50, before and after leaching, respectively. As-injected specimens, as shown in Figure 4(a), displayed smooth surfaces with wave-like textures as they were covered up by polymeric binders. In the specimens with high alumina contents, e.g., A30 to A50, islands of particulate features can be observed on the surface, and were confirmed by EDS to be alumina. After leaching, the specimens displayed rough surfaces with particulate textures as shown in Figure 4(b). It is noted that leached specimens with low alumina content appear more planar. Those with high alumina contents reveal scattered surface pits.

3.2 Density measurement

In thermal debinding and sintering process, PVB was eliminated from the specimens and the remaining ceramic components fused together. Bulk density data of the sintered samples are plotted as percentage of theoretical density against alumina content in Figure 5(a). Sample porosity data are also depicted in the same plot. Bulk density of A0 and A10 were the highest at 91% of theoretical value. As the alumina content was increased, the bulk density values gradually declined. This is in agreement with porosity result; A0 and A10 were the least porous, and the porosity increased with increasing alumina content. A50 yielded the lowest bulk density and the highest porosity. The porosity and density of sintered specimens also reflected in the specimen dimensions after sintering. Given that all as-injected specimens were of the same size, A0 and A10 shrank down the most and became denser than other conditions as shown in Figure 5(b). The other specimens with high porosity remain large after sintering.

The high porosity values of the specimens with large alumina addition could be attributed to hollowing morphology after leaching (Figure 4(b)) and the powder size difference. The median value of particle size distribution (D50) of zirconia and alumina powders, characterized by a laser particles size distribution analyzer, were 3.2 μm and 1.28 μm, respectively. At high alumina content, this size contrast could affect the sintering of each constituent. Another factor might be the sintering temperature. To accommodate the majority zirconia phase, the composite specimens were sintered at 1450°C, which was lower than typical alumina sintering temperature, around 1600°C. In the specimens with high alumina content, the alumina portion might not have been sintered fully such that more porosity remained.

3.3 Microstructure and surface chemical composition

Microstructural observation as well as surface chemical composition were performed on fracture surfaces of sintered specimens using SEM and EDS. The morphology images are shown in Figure 6(a). The images of fracture surfaces of A0 and A10, ceramic particles appeared to be compacted and fused well together, creating large unified areas. With more alumina content in A20, the ceramic particles appeared partly isolated and small pores scattered throughout the surface. In A30, A40 and A50 images, ceramic particles were mostly isolated and appear not fully sintered. The higher the alumina content, the more porosity observed on the surfaces. This result is in agreement with the density measurement. The EDS analyses of the fracture surfaces are depicted in Figure 6(b). The specimens contained zirconium, aluminum and oxygen. As expected, the aluminum content detected via EDS increased proportionally to the amount of alumina added in the prepared specimens.

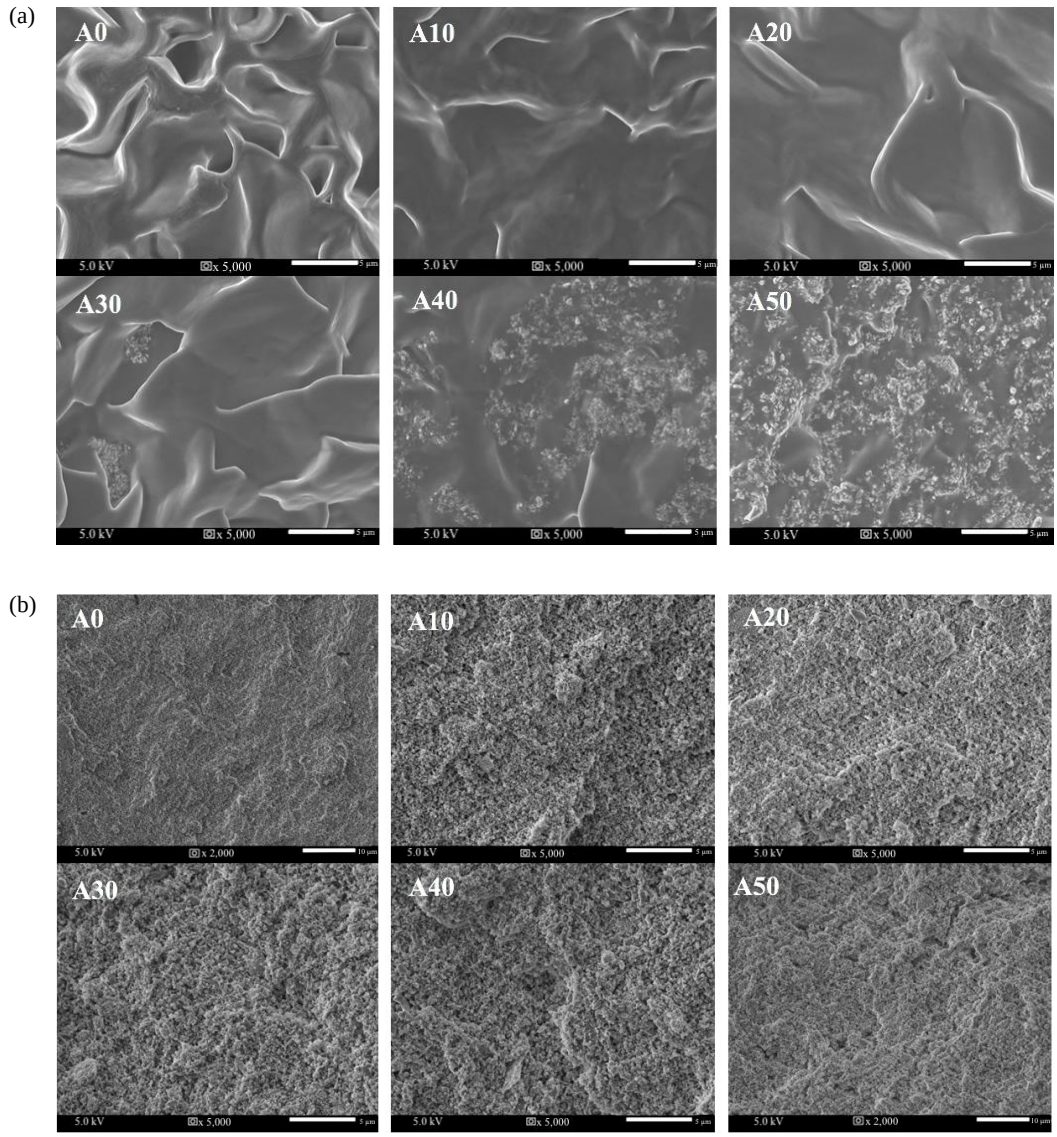

Figure 4. (a) Surface morphology of as-injected zirconia-alumina composite specimens, A0 to A50. (b) Surface morphology of water-debinded zirconia-alumina composite specimens, A0 to A50.

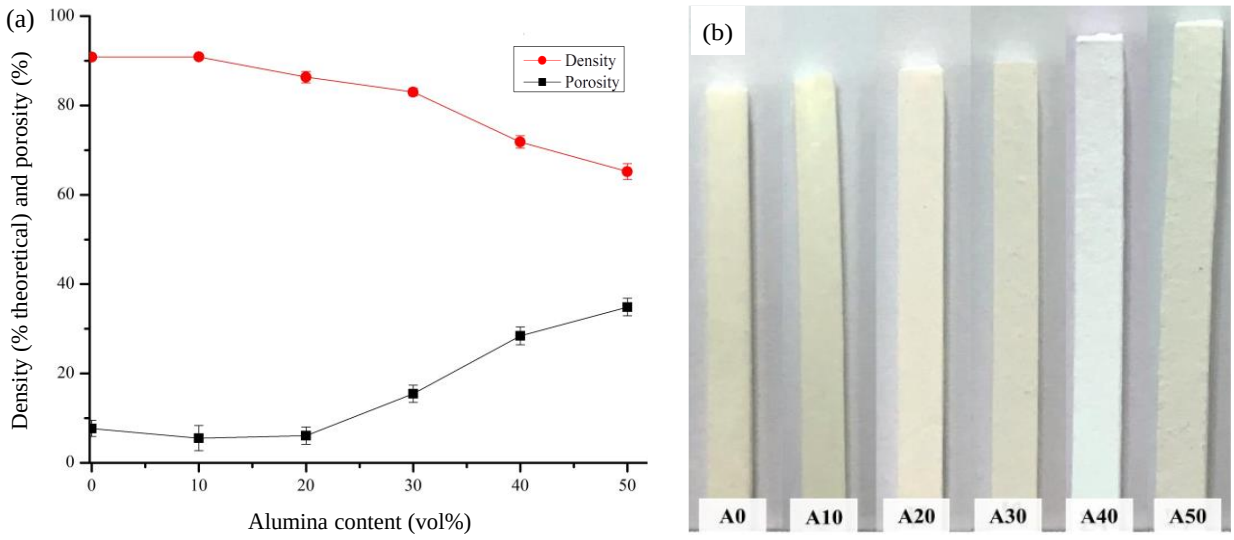

Figure 5. (a) Bulk density and porosity of sintered zirconia-alumina composite samples versus alumina content. (b) variation of specimen size after sintering.

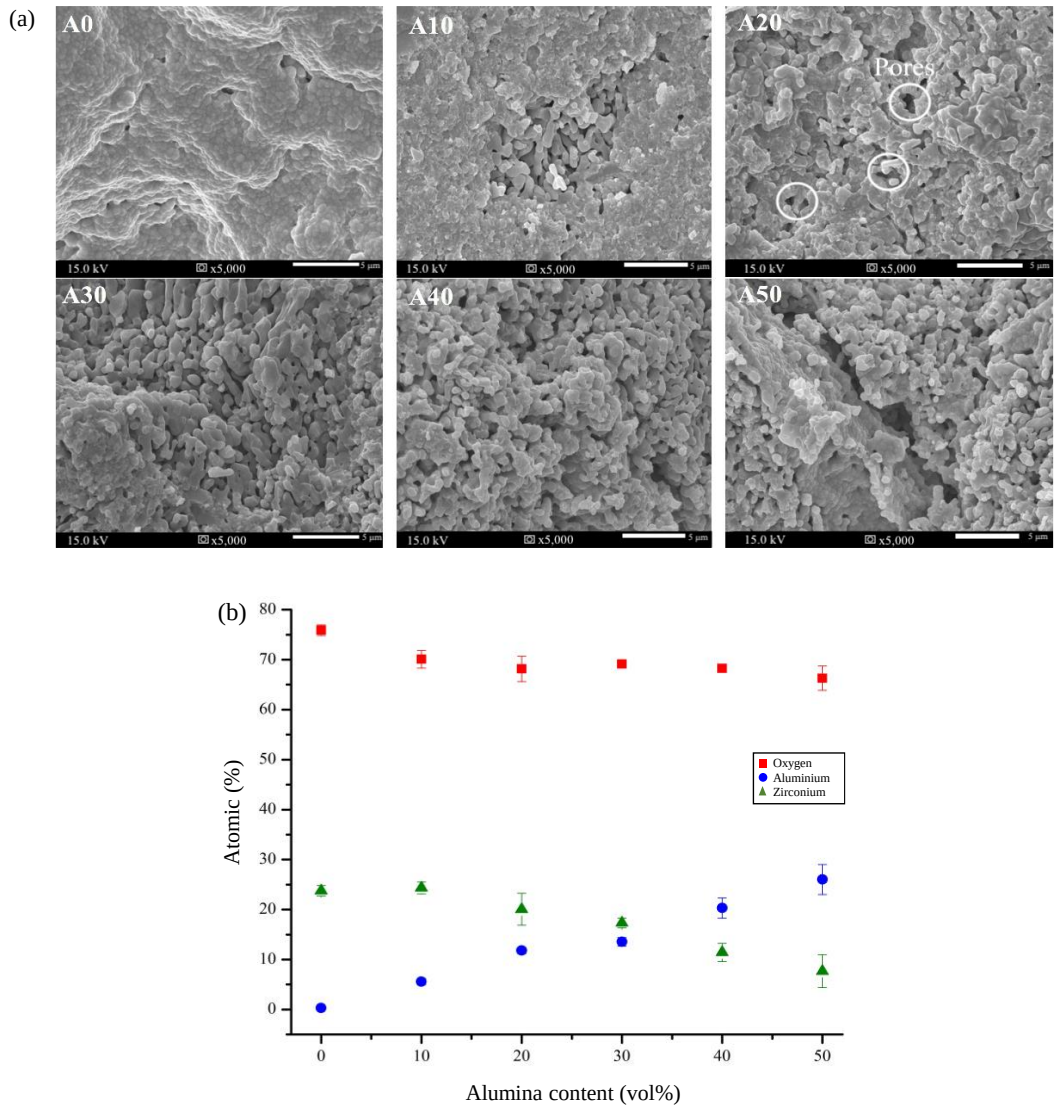

Figure 6. Morphological SEM images of the fracture surfaces for sintered composite specimens with varying alumina content (a), and chemical composition obtained from EDS of the fracture surfaces (b).

3.4 X-ray diffraction analysis (XRD)

Phase composition of the composite specimens were characterized using XRD. XRD patterns of sintered specimens with varying alumina are shown in Figure 7(a). The phases that could be identified include tetragonal zirconia (ICSD 066787), monoclinic zirconia (ICSD 062993) and aluminum oxide (ICSD 60419). A0 specimen which contained no alumina exhibited only tetragonal zirconia phase with prominent peaks corresponding to (101), (112) and (211) and reflections. With alumina added, in A10 to A50, small aluminum oxide peaks could be detected. In A10 the alumina peaks are very small such that the pattern of A10 is amplified in Figure 7(b) to make the alumina peaks more noticeable. Evident alumina reflections included (104), (113), (024) and (116). With more alumina addition, the alumina peaks became higher. The composite system did not form any new zirconia-alumna phase. Each component, alumina and zirconia, existed as separate phases, conforming to the phase behavior of zirconia alumina system. With alumina addition of at least 20 vol%, in A20 to A50, monoclinic zirconia phase also existed, as monoclinic ($\bar{1}11$) and (111) peaks became more apparent with increasing alumina content. It was found that with enough alumina addition, tetragonal zirconia phase was no longer stabilized completely. From the microstructure analysis, the composite samples with 20 vol% alumina and above contained large porosity. These porous structures could lead to early tetragonal to monoclinic transformation. This result is similarly to what observed in previous study by Kern *et al.* [8]

3.5 Flexural properties

Flexural modulus and flexural strength data of the sintered specimens at varying alumina content are depicted graphically in Figure 8. Flexural modulus was about 40 GPa for pure zirconia specimens, A0. With small addition of alumina in A10, the flexural modulus rose up to 46 GPa, which was the largest value among all

specimen conditions. When more alumina was added, in A20 to A50, the modulus gradually declined to the lowest value at 50 vol% alumina. The obtained flexural modulus values are the first reported values for powder injected zirconia-alumina composites [3,6,11]. Compared to flexural modulus of zirconia-alumina systems formed by other fabrication methods, the flexural modulus values from the current study are lower since the technique allows less compaction.

The obtained current result is also different from previous studies that employed other fabrication methods, most of which reported enhanced modulus with increasing alumina content [3,6,7]. According to mixture rule in fundamental composite theory, adding alumina should enhance modulus of the composites, since alumina's elastic modulus is higher than zirconia's. But from the experiment result, this is true only at low alumina addition. At higher alumina content, the stiffening mechanism by alumina was weakened by porous microstructure. With scattered pores, the composite specimens were not well integrated such that the modulus mixing rule no longer applied. Yet, the porosity, having a direct effect on modulus, can be considered as another component in the composites. The more the porosity the lower the modulus.

Flexural strength varied with the alumina content similarly to how modulus did. Flexural strength of pure zirconia specimens, A0, was averaged to be 185 MPa. For A10, condition with 10 vol% alumina addition, the flexural strength was about 290 MPa, the highest value among all specimen conditions. With further addition of alumina, in A20, A30, A40 and A50, the flexural strengths were lower, having values ranging between 60 and 120 MPa. Similar to flexural modulus trend, the flexural strength decreased when alumina content was high, and were in correlation with porosity. A10 which contained lowest porosity exhibited largest value of flexural strength. When alumina content was more than 10 vol%, the flexural strength reduced to a lower range. Such reduction, which was not in proportion with alumina addition, could be attributed to the existence of pores in the specimens. The existence of pores, regardless of porosity fraction, facilitated crack propagation and led to failure at low strength. This contrasted to how porosity amount proportionally affected the flexural modulus values. Another factor that could lead to deteriorated mechanical properties at high alumina addition was the emergence of monoclinic phase, which could cause structural distortion and lattice strain.

The flexural strength of powder injected zirconia-alumina composites in this study can be compared to similar systems. Previous studies on pure zirconia and zirconia-toughened alumina fabricated via powder injection molding reported increasing flexural strength with increasing powder loading and varied with binder types. The flexural strength values for the pure zirconia ranged from 20-610 MPa [19,29] and for the zirconia-toughened alumina were around 260-330 MPa [23]. In other forming methods, the zirconia-alumina composites prepared by uniaxial pressing process yielded higher flexural strength, around 470-1900 MPa because the specimens could attain relative density up to 99%. Even though the flexural strength obtained in the current investigation is not as high, the value is still superior to other materials. Moreover, powder injection molding technique is advantageous that the specimens can be fabricated into small, complex and near-net shape, unlike those obtained from conventional methods [7,8].

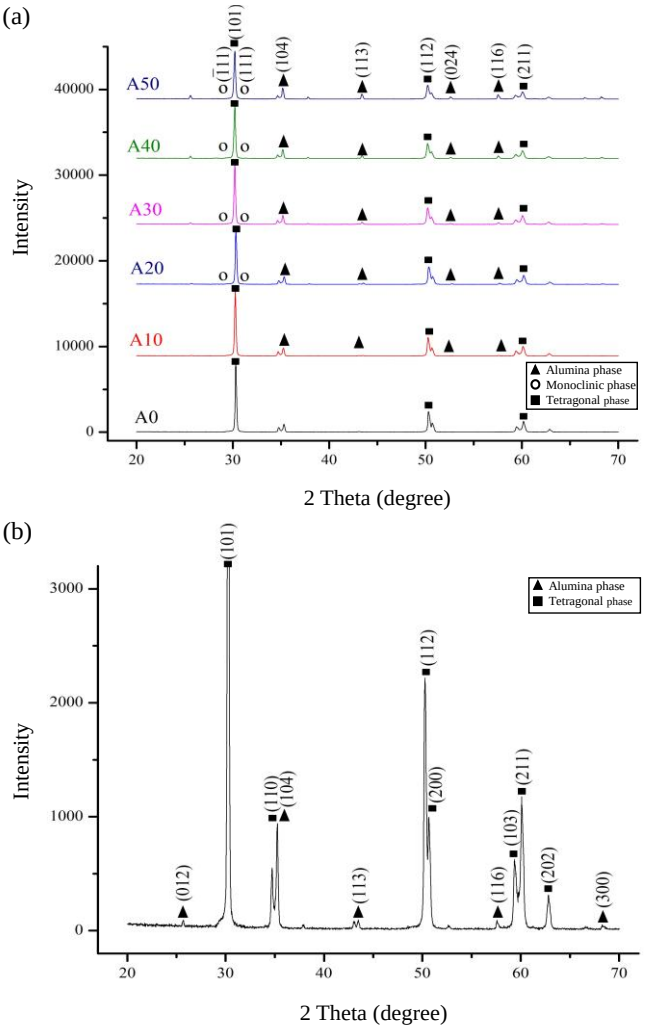

Figure 7. (a) XRD patterns for zirconia-alumina composite samples, A0 to A50, with increasing alumina content. (b) amplified XRD pattern for A10 illustrates the emergence of alumina.

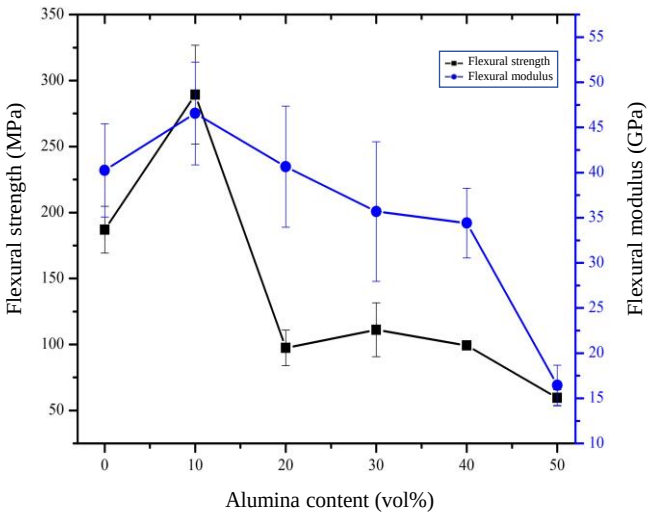

Figure 8. Flexural modulus (right) and flexural strength (left) of zirconia-alumina composite.

4. Conclusions

This study is the first to fabricate zirconia-alumina composites via powder injection molding with alumina content varying from 0 to 50 vol%, using fixed powder-to-binder ratio at 32:68 by volume. The fabrication process utilized environmental-friendly binders, PEG and PVB, which can be removed by water and heat respectively. The water debinding process, in which PEG was affirmed to be completely leached out after 24 h, created porous microstructure which allowed PVB to be removed in the thermal debinding process. The samples with alumina content higher than 10 vol% contained substantial porosity which led to declining flexural properties. The condition with 10 vol% alumina yielded highest bulk density at 91% of the theoretical value, lowest porosity and optimum flexural properties with flexural strength of 290 MPa and flexural modulus of 46 GPa. The small addition of alumina sufficiently reinforced zirconia matrix without excessive modification of microstructure and constituent phases. Despite the lower mechanical properties obtained in this study compared to previous studies accomplished via other fabrication techniques, the current work validates the potential of using PIM as a fabrication of zirconia-alumina composites into specified shapes. For future work, other factors such as powder size, powder-to-binder ratio, and sintering temperature can be investigated to better enhance the properties of the composites.

5. Acknowledgements

This research work was supported by Srinakharinwirot University, Thailand, grant number 72/2562.

References

[1] J. Wang, and M.J. Edirisinghe, "Ceramic Injection Molding," in *Reference Module in Materials Science and Materials Engineering*: Elsevier, 2016.

[2] J. Chevalier, "What future for zirconia as a biomaterial?," *Biomaterials*, vol. 27(4), pp. 535-543, 2006.

[3] M. Fornabaio, P. Palmero, R. Traverso, C. Esnouf, H. Reveron, J. Chevalier, and L. Montanaro "Zirconia-based composites for biomedical applications: Role of second phases on composition, microstructure and zirconia transformability," *Journal of the European Ceramic Society*, vol. 35(14), pp. 4039-4049, 2015.

[4] S. Pieralli, R.-J. Kohal, E. Lopez Hernandez, S. Doerken, and B. C. Spies, "Osseointegration of zirconia dental implants in animal investigations: A systematic review and meta-analysis," *Dental Materials*, vol. 34(2), pp. 171-182, 2018.

[5] K. Sivaraman, A. Chopra, A. I. Narayan, and D. Balakrishnan, "Is zirconia a viable alternative to titanium for oral implant? A critical review," *Journal of Prosthodontic Research*, vol. 62(2), pp. 121-133, 2018.

[6] A. Celli, A. Tucci, L. Esposito, and C. Palmonari, "Fractal analysis of cracks in alumina–zirconia composites," *Journal of the European Ceramic Society*, vol. 23(3), pp. 469-479, 2003.

[7] S. Sequeira, M. H. Fernandes, N. Neves, and M. M. Almeida, "Development and characterization of zirconia–alumina composites for orthopedic implants," *Ceramics International*, vol. 43(1), Part A, pp. 693-703, 2017.

[8] F. Kern, and R. Gadow, "Alumina toughened zirconia from yttria coated powders," *Journal of the European Ceramic Society*, vol. 32(15), pp. 3911-3918, 2012.

[9] A. Nevarez-Rascon, A. Aguilar-Elguezabal, E. Orrantia, and M.H. Bocanegra-Bernal, "Compressive strength, hardness and fracture toughness of Al_2O_3 whiskers reinforced ZTA and ATZ nano-composites: Weibull analysis," *International Journal of Refractory Metals and Hard Materials*, vol. 29(3), pp. 333-340, 2011.

[10] H.L.C. Pulgarin, and M.P. Albano, "Sintering, microstrusture and hardness of different alumina–zirconia composites," *Ceramics International*, vol. 40(4), pp. 5289-5298, 2014.

[11] H.L.C. Pulgarin, and M.P. Albano, "Three different alumina–zirconia composites: Sintering, microstructure and mechanical properties," *Materials Science and Engineering: A*, vol. 639, pp. 136-144, 2015.

[12] B. Stawarczyk, M. Özcan, L. Hallmann, A. Ender, A. Mehl, and C. Hämmerlet, "The effect of zirconia sintering temperature on flexural strength, grain size, and contrast ratio," *Clinical oral investigations*, vol. 17, 2012.

[13] F. Allaire, B. R. Marple, and J. Boulanger, "Injection molding of submicrometer zirconia: blend formulation and rheology," *Ceramics International*, vol. 20(5), pp. 319-325, 1994.

[14] S. Chauoon, M. Meepho, N. Chuankrerkkul, S. Chaianansutcharit, and R. Pornprasertsuk, "Fabrication of yttria stabilized zirconia thin films on powder-injected anode substrates by electrophoretic deposition technique for solid oxide fuel cell application," *Thin Solid Films*, vol. 660, pp. 741-748, 2018.

[15] A. Faes, H. Girard, A. Zryd, Z. Wuillemin, and J. Van herle, "Fabrication of structured anode-supported solid oxide fuel cell by powder injection molding," *Journal of Power Sources*, vol. 227, pp. 35-40, 2013.

[16] R. Martin, M. Vick, M. Kelly, J.P. de Souza, R.K. Enneti, and S. V. Atre, "Powder injection molding of a mullite–zirconia composite," *Journal of Materials Research and Technology*, vol. 2(3), pp. 263-268, 2013.

[17] L. Liu, X.L. Ni, H.Q. Yin, and X.H. Qu, "Mouldability of various zirconia micro gears in micro powder injection moulding," *Journal of the European Ceramic Society*, vol. 35(1), pp. 171-177, 2015.

[18] J. Xiao, W. Cai, J. Liu, and M. Liu, "A novel low-pressure injection molding technique for fabricating anode supported solid oxide fuel cells," *International Journal of Hydrogen Energy*, vol. 39(10), pp. 5105-5112, 2014.

[19] F. Mohd Foudzi, N. Muhamad, A. Bakar Sulong, and H. Zakaria, "Yttria stabilized zirconia formed by micro ceramic injection molding: Rheological properties and debinding effects on the sintered part," *Ceramics International*, vol. 39(3), pp. 2665-2674, 2013.

[20] J. He, Z. Shao, D.F. Khan, H. Yin, S. Elder, Q. Zheng, and X. Qu, "Investigation of inhomogeneity in powder injection molding of nano zirconia," *Powder Technology*, vol. 328, pp. 207-214, 2018.

[21] J. Wen, W. Liu, Z. Xie, C. Lou, and X. Yang, "Effects of the binder compositions on the homogeneity of ceramic injection molded compacts," *Ceramics International*, vol. 44(3), pp. 3218-3225, 2018.

[22] S. Md Ani, A. Muchtar, N. Muhamad, and J. A. Ghani, "Fabrication of zirconia-toughened alumina parts by powder injection molding process: Optimized processing parameters," *Ceramics International*, vol. 40(1), Part A, pp. 273-280, 2014.

[23] N. Chuankrerkkul, K. Somton, T. Wonglom, K. Dateraksa, and P. Laoratanakul, "Physical and mechanical properties of zirconia toughened alumina (ZTA) composites fabricated by powder injection moulding," *Chiang Mai Journal of Science*, vol. 43, pp. 375-380, 2016.

[24] F. Sommer, H. Walcher, F. Kern, M. Maetzig, and R. Gadow, "Influence of feedstock preparation on ceramic injection molding and microstructural features of zirconia toughened alumina," *Journal of the European Ceramic Society*, vol. 34(3), pp. 745-751, 2014.

[25] N. Chuankrerkkul, R. Charoenkijmongkol, P. Somboonthanasarn, C. Auechalitanukul, and R.C. McCuiston, "Microstructure and properties of zirconia toughened alumina fabricated by powder injection moulding," *Key Engineering Materials*, vol. 659, pp. 116-120, 2015.

[26] V.A. Krauss, A.A.M. Oliveira, A.N. Klein, H.A. Al-Qureshi, and M.C. Fredel, "A model for PEG removal from alumina injection moulded parts by solvent debinding," *Journal of Materials Processing Technology*, vol. 182(1), pp. 268-273, 2007.

[27] X. Yang, Z. Xie, G. Liu, and Y. Huang, "Dynamics of Water Debinding in Ceramic Injection Moulding," *Advances in Applied Ceramics - ADV APPL CERAM*, vol. 108, pp. 295-300, 2009.

[28] W. Liu, J. Wen, Z. Xie, and X. Yang, "Powder modification mechanism, effects of binder compositions on the thermal behavior, and the mechanical properties of the ceramic injection molded system," *Ceramics International*, vol. 44(5), pp. 5646-5651, 2018.

[29] Z. Xie, J. Luo, X. Wang, J. Li, and Y. Huang, "The effect of organic vehicle on the injection molding of ultra-fine zirconia powders," *Materials & Design*, vol. 26(1), pp. 79-82, 2005.